

IEEE TRANSACTIONS ON GEOSCIENCE AND REMOTE SENSING

A PUBLICATION OF THE IEEE GEOSCIENCE AND REMOTE SENSING SOCIETY



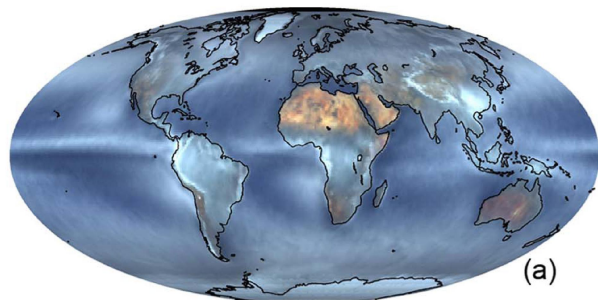
JULY 2016

VOLUME 54

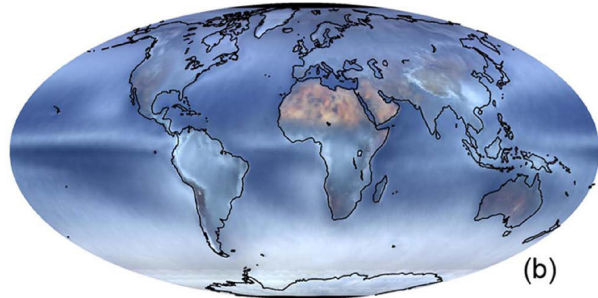
NUMBER 7

IGRSD2

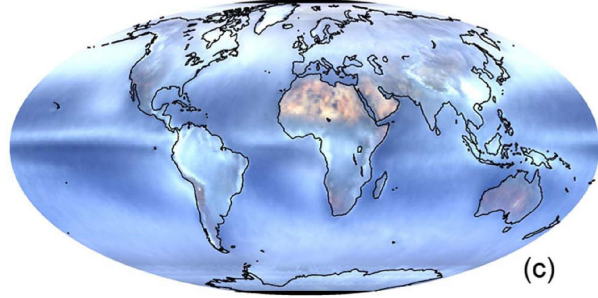
(ISSN 0196-2892)



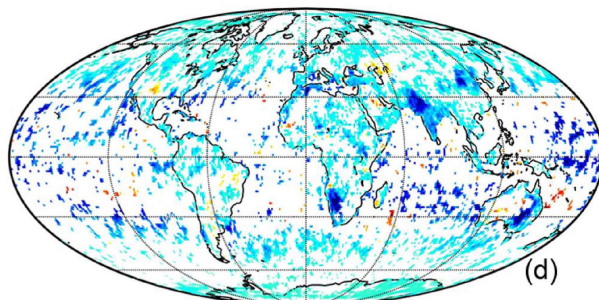
(a)



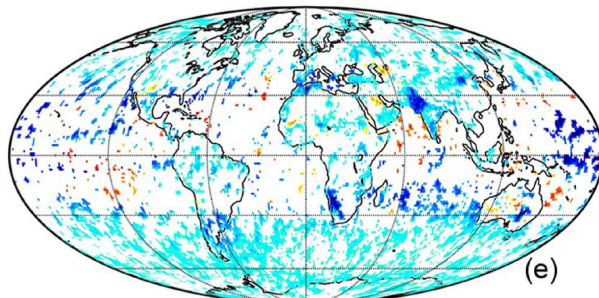
(b)



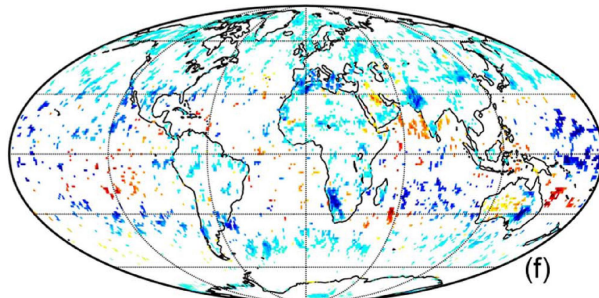
(c)



(d)



(e)



(f)

RGB Mean

-10 -5 0 5 10 [%/decade]

Fifteen-year-averaged RGB images of the Earth from MISR nadir (AN) and two oblique cameras (DA and DF), along with significant trends in color changing of the Earth.

IEEE TRANSACTIONS ON GEOSCIENCE AND REMOTE SENSING

A PUBLICATION OF THE IEEE GEOSCIENCE AND REMOTE SENSING SOCIETY



JULY 2016

VOLUME 54

NUMBER 7

IGRSD2

(ISSN 0196-2892)

PAPERS

Atmosphere

Range Imaging of E-Region Field-Aligned Irregularities by Using a Multifrequency Technique: Validation and Initial Results	J.-S. Chen, Y.-H. Chu, C.-L. Su, H. Hashiguchi, and Y. Li	3739
Ozone Profile Retrievals From the Cross-Track Infrared Sounder	P. Ma, L. Chen, Z. Wang, S. Zhao, Q. Li, M. Tao, and Z. Wang	3985
A Weather Radar Simulator for the Evaluation of Polarimetric Phased Array Performance	A. D. Byrd, I. R. Ivić, R. D. Palmer, B. M. Isom, B. L. Cheong, A. D. Schenkman, and M. Xue	4178

Oceans

An Improved Singularity Analysis for ASCAT Wind Quality Control: Application to Low Winds	W. Lin, M. Portabella, A. Turiel, A. Stoffelen, and A. Verhoef	3890
---	--	------

Electromagnetics

Multimode Coherent Pattern in Bistatic Scattering From Randomly Corrugated Surfaces With Irregular Grooves at L-Band	P. Xu, K.-S. Chen, Y. Liu, and Z.-W. Li	4143
--	---	------

Hyperspectral Data Processing

Recursive Orthogonal Projection-Based Simplex Growing Algorithm	H.-C. Li and C.-I. Chang	3780
Estimating the Intrinsic Dimension of Hyperspectral Images Using a Noise-Whitened Eigengap Approach	A. Halimi, P. Honeine, M. Kharouf, C. Richard, and J.-Y. Tourneret	3811
Discriminative Multiple Kernel Learning for Hyperspectral Image Classification	Q. Wang, Y. Gu, and D. Tuia	3912
Biobjective Nonnegative Matrix Factorization: Linear Versus Kernel-Based Models	F. Zhu and P. Honeine	4012
Hyperspectral Image Classification via Basic Thresholding Classifier	M. A. Toksoz and İ. Ulusoy	4039
Efficient Multiple-Feature Learning-Based Hyperspectral Image Classification With Limited Training Samples	C. Zhao, X. Gao, Y. Wang, and J. Li	4052
Hyperspectral Local Intrinsic Dimensionality	L. Drumetz, M. A. Veganzones, R. Marrero Gómez, G. Tochon, M. D. Mura, G. A. Licciardi, C. Jutten, and J. Chanussot	4063
Sparse and Low-Rank Graph for Discriminant Analysis of Hyperspectral Imagery	W. Li, J. Liu, and Q. Du	4094
Automatic Object-Based Hyperspectral Image Classification Using Complex Diffusions and a New Distance Metric	A. Zehtabian and H. Ghassemian	4106

(Contents Continued on Page 3738)

Orthogonal Nonnegative Matrix Factorization Combining Multiple Features for Spectral–Spatial Dimensionality Reduction of Hyperspectral Imagery	J. Wen, J. E. Fowler, M. He, Y.-Q. Zhao, C. Deng, and V. Menon	4272
Image Processing and Analysis		
Global and Local Saliency Analysis for the Extraction of Residential Areas in High-Spatial-Resolution Remote Sensing Image	L. Zhang, A. Li, Z. Zhang, and K. Yang	3750
Learning-Based Superresolution Land Cover Mapping	F. Ling, Y. Zhang, G. M. Foody, X. Li, X. Zhang, S. Fang, W. Li, and Y. Du	3794
A Superresolution Land-Cover Change Detection Method Using Remotely Sensed Images With Different Spatial Resolutions	X. Li, F. Ling, G. M. Foody, and Y. Du	3822
Fusion Methods for Land Surface Emissivity and Temperature Retrieval of the Landsat Data Continuity Mission Data	H. Emami, A. Safari, and B. Mojarradi	3842
Remote Sensing Image Classification Using Attribute Filters Defined Over the Tree of Shapes	G. Cavallaro, M. D. Mura, J. A. Benediktsson, and A. Plaza	3899
An Operational Radiometric Landsat Preprocessing Framework for Large-Area Time Series Applications	D. Frantz, A. Röder, M. Stellmes, and J. Hill	3928
Improving the Spatial Resolution of Land Surface Phenology by Fusing Medium- and Coarse-Resolution Inputs	D. Frantz, M. Stellmes, A. Röder, T. Udelhoven, S. Mader, and J. Hill	4153
Microwave Radiometry		
Tropical Convective Cloud Characterization Using Ground-Based Microwave Radiometric Observations	R. Renju, C. Suresh Raju, N. Mathew, N. V. P. Kirankumar, and K. Krishna Moorthy	3774
An Empirical Model for Television Frequency Interference Correction of AMSR2 Data Over Ocean Near the U.S. and Europe	X. Tian and X. Zou	3856
Radar Systems		
Moving-Target Tracking by Cognitive RF Stealth Radar Using Frequency Diverse Array Antenna	W.-Q. Wang	3764
Investigation of SMAP Fusion Algorithms With Airborne Active and Passive L-Band Microwave Remote Sensing	C. Montzka, T. Jagdhuber, R. Horn, H. R. Bogena, I. Hajnsek, A. Reigber, and H. Vereecken	3878
Generalized Terrain Topography in Radar Scattering Models	M. S. Burgin, U. K. Khankhoje, X. Duan, and M. Moghaddam	3944
Synthetic Aperture Radar		
Polarimetric SAR Change Detection With the Complex Hotelling–Lawley Trace Statistic	V. Akbari, S. N. Anfinsen, A. P. Doulgeris, T. Eltoft, G. Moser, and S. B. Serpico	3953
Use of Doppler Parameters for Ship Velocity Computation in SAR Images	A. Renga and A. Moccia	3995
A Frequency-Domain Imaging Algorithm for Highly Squinted SAR Mounted on Maneuvering Platforms With Nonlinear Trajectory	Z. Li, M. Xing, Y. Liang, Y. Gao, J. Chen, Y. Huai, L. Zeng, G.-C. Sun, and Z. Bao	4023
Polarimetric SAR Image Filtering Based on Patch Ordering and Simultaneous Sparse Coding	B. Xu, Y. Cui, B. Zuo, J. Yang, and J. Song	4079
Simultaneous Stationary Scene Imaging and Ground Moving Target Indication for High-Resolution Wide-Swath SAR System	X. Li, M. Xing, X.-G. Xia, G.-C. Sun, Y. Liang, and Z. Bao	4224
Spherical Symmetry of Complex Stochastic Models in Multivariate High-Resolution PolSAR Images	L. Pralon, G. Vasile, M. D. Mura, A. Anghel, and J. Chanussot	4250
Evaluation of ICA-Based ICTD for PolSAR Data Analysis Using a Sliding Window Approach: Convergence Rate, Gaussian Sources, and Spatial Correlation	L. Pralon, G. Vasile, M. D. Mura, J. Chanussot, and N. Besic	4262
SAR Image Segmentation Based on Hierarchical Visual Semantic and Adaptive Neighborhood Multinomial Latent Model	F. Liu, Y. Duan, L. Li, L. Jiao, J. Wu, S. Yang, X. Zhang, and J. Yuan	4287
Statistical Modeling of PMA Detector for Ship Detection in High-Resolution Dual-Polarization SAR Images	G. Gao, Y. Luo, K. Ouyang, and S. Zhou	4302
A New Semiautomated Detection Mapping of Flood Extent From TerraSAR-X Satellite Image Using Rule-Based Classification and Taguchi Optimization Techniques	B. Pradhan, M. S. Tehrany, and M. N. Jebur	4331
Interferometric Processing of ScanSAR Data Using Stripmap Processor: New Insights From Coregistration	C. Liang and E. J. Fielding	4343
Global Navigation Satellite System		
Open-Loop Tracking of Rising and Setting GPS Radio-Occultation Signals From an Airborne Platform: Signal Model and Error Analysis	K.-N. Wang, J. L. Garrison, U. Acikoz, J. S. Haase, B. J. Murphy, P. Muradyan, and T. Lulich	3967

Lidar Systems		
Automated Detection of Three-Dimensional Cars in Mobile Laser Scanning Point Clouds Using DBM-Hough-Forests	Y. Yu, J. Li, H. Guan, and C. Wang	4130
Fusion of LiDAR Orthowaveforms and Hyperspectral Imagery for Shallow River Bathymetry and Turbidity Estimation	Z. Pan, C. L. Glennie, J. C. Fernandez-Diaz, C. J. Legleiter, and B. Overstreet	4165
A Hierarchical Approach to Three-Dimensional Segmentation of LiDAR Data at Single-Tree Level in a Multilayered Forest	C. Paris, D. Valduga, and L. Bruzzone	4190
Marker-Free Registration of Forest Terrestrial Laser Scanner Data Pairs With Embedded Confidence Metrics	D. Kelbe, J. van Aardt, P. Romanczyk, M. van Leeuwen, and K. Cawse-Nicholson	4314
UV/Visible/Infrared Imagers		
Small Infrared Target Detection Based on Weighted Local Difference Measure	H. Deng, X. Sun, M. Liu, C. Ye, and X. Zhou	4204
Satellite Systems		
Direction-of-Arrival Estimation of VHF Signals Recorded on the International Space Station and Simultaneous Observations of Optical Lightning	H. Kikuchi, T. Morimoto, M. Sato, T. Ushio, M. Kikuchi, A. Yamazaki, M. Suzuki, R. Ishida, Y. Sakamoto, and Z. Kawasaki	3868
Global Estimates for High-Spatial-Resolution Clear-Sky Land Surface Upwelling Longwave Radiation From MODIS Data	J. Cheng and S. Liang	4115
FLEX End-to-End Mission Performance Simulator	J. Vicent, N. Sabater, C. Tenjo, J. R. Acarreta, M. Manzano, J. P. Rivera, P. Jurado, R. Franco, L. Alonso, J. Verrelst, and J. Moreno	4215
Regional Changes in Earth's Color and Texture as Observed From Space Over a 15-Year Period	G. Zhao, L. Di Girolamo, D. J. Diner, C. J. Bruegge, K. J. Mueller, and D. L. Wu	4240
Robust Approach for Recovery of Rigorous Sensor Model Using Rational Function Model	W. Huang, G. Zhang, and D. Li	4355
ANNOUNCEMENTS		
Call for Papers—IEEE JOURNAL OF SELECTED TOPICS IN APPLIED EARTH OBSERVATION AND REMOTE SENSING Issue on the IGARSS 2016 Symposium		4363

About the Cover: Earth-Observing satellites provide global observations of many geophysical variables. As these variables are derived from measured radiances, the underlying radiance data are the most reliable sources of information for change detection. The radiance data collected by the Multi-angle Imaging SpectroRadiometer (MISR) reveal significantly large regional shifts in color and texture in the past 15 years. These large regional trends cannot be explained either by uncertainties in radiometric calibration or variability in total or spectral solar irradiance; hence they reflect changes internal to Earth's climate system. This figure shows the 15-year-mean true color composites images of the Earth at both nadir and oblique views along with significant trends in color shift. Regions with negative trends become redder over time, while regions with positive trends become bluer. For more information please see "Regional Changes in Earth's Color and Texture as Observed From Space Over a 15-Year Period," by Zhao *et al.*, which begins on page 4240.